Conference materials
UDC 523.985.3
DOI: https://doi.org/10.18721/JPM.161.275

X-ray radiation of partially occulted solar flare of May 13, 2013

E.P. Ovchinnikova[1]✉,

[1]Ioffe Institute, St. Petersburg, Russia

✉elfimovaevgeniya@gmail.com

Abstract. The X-ray emission of the SOL2013-05-13T02:12 X1.7-GOES-class flare registered by the RHESSI spectrometer was analyzed. Various models of fitting the X-ray spectrum are applied. The following radiation models are considered: a two-temperature hot plasma model, a combination of a thin target model and a single-temperature plasma model, a combination of a bremsstrahlung model of a thick target and quasi-thermal radiation of a single-temperature plasma. Their validity to the spectra for this event is discussed. Plasma parameters are evaluated: emission measures, temperatures and density.

Keywords: Sun, solar flares, X-rays, RHESSI, thin target, thick target, bremsstrahlung.

Citation: Ovchinnikova E.P., X-ray radiation of partially occulted solar flare of May 13, 2013, St. Petersburg State Polytechnical University Journal. Physics and Mathematics. 16 (1.2) (2023) 492–498. DOI: https://doi.org/10.18721/JPM.161.275

Материалы конференции
УДК 523.985.3
DOI: https://doi.org/10.18721/JPM.161.275

Рентгеновское излучение частично затенненой солнечной вспышки 13 мая 2013

Е.П. Овчинникова [1] ✉

[1] Физико-технический институт им. А.Ф. Иоффе РАН, Санкт-Петербург, Россия

✉elfimovaevgeniya@gmail.com

Аннотация. Проведен анализ рентгеновского излучения вспышки X-1.7GOES класса SOL13-05-2013T02:12, зарегистрированной спектрометром RHESSI. Анализируются модели спектров рентгеновского излучения. Рассматриваются различные модели излучения: двухтемпературная модель горячей плазмы, совокупность модели тонкой мишени и модели однотемпературной плазмы, совокупность модели тормозного излучения (bremsstrahlung) толстой мишени и квазитеплового излучения однотемпературной плазмы. Обсуждается возможность их реализации для данного события. Проводится оценка параметров плазмы: меры эмиссии, температуры и концентрации.

Ключевые слова: Солнце, солнечные вспышки, рентгеновское излучение, RHESSI, модель тонкой мишени, модель толстой мишени, тормозное излучение._

Ссылка при цитировании: Овчинникова Е.П. Рентгеновское излучение частично затенненой солнечной вспышки 13 мая 2013 // Научно-технические ведомости СПбГПУ. Физико-математические науки. 2023. Т. 16. № 1.2. С. 492–498. DOI: https://doi.org/10.18721/JPM.161.275

Introduction

During solar flares, a large amount of stored free energy of the magnetic field is released in the form of heated plasma and charged particles accelerated to energies of at least hundreds of keV. Super-hot plasma with a temperature of tens of MK and accelerated particles emit in the range from radio to gamma-rays [1]. At the same time, the possible acceleration processes have a different nature and can occur in several stages [2]. Subsequently, charged particle beams, during propagation in open and closed magnetic field configurations, undergo significant transformations in the spectrum, pitch-angular distribution due to the influence of many competing processes: secondary acceleration, Coulomb scattering, induced return current, magnetic mirroring, turbulence, magnetic fluctuations, magnetohydrodynamic waves etc [3, 4]. Plasma density and temperature in flaring magnetic structures change as a result of the evaporation effect, the transformation of the magnetic fields themselves [5–7]. All these effects and many others dramatically distort the spectra of accelerated particles, the distribution of temperature and plasma density along the flare loops. Due to the complexity of constructing numerical models that could take into account the listed transport, acceleration, diffusion effects, in the field of spectral analysis of flare phenomena, it is customary to use approximate analysis methods such as one or two temperature models of hot plasma, models of thin, thick and warm targets [8–11]. The use of simplified models can cause ambiguity in the results of the analysis. In this paper, the event is considered which is interesting because due to the partially occulted footpoints of the magnetic arcade, it is possible to observe a coronal source in the hard X-ray range. The analysis of spectra of coronal sources in such events is particularly interesting for assessing the applicability of simplified models of approximation of spectra, since the plasma density during the flare in the coronal part can vary within a sufficiently wide range, which can lead to the appearance of conditions for the implementation of the thick target and thin target models for different populations of accelerated electrons.

The flare SOL2013-05-13T02:12

The SOL2013-05-13T02:12 flare occurred in the active region AR11748, which was near the Sun's limb on the invisible side, the coronal part and partially the chromospheric part of the magnetic field structure was visible in X-Rays and EUV by The Reuven Ramaty High-Energy Solar Spectroscopic Imager (RHESSI) [12] and by The Atmospheric Imaging Assembly (AIA) on the Solar Dynamics Observatory (SDO) [13]. We will call such an event a partially occulted flare [14], because sometimes radiation from the chromospheric regions of the flare arcade is observed (Fig. 1,*a*). The X-ray source at the looptop is visible in the range of 6-20 keV throughout the entire flare.

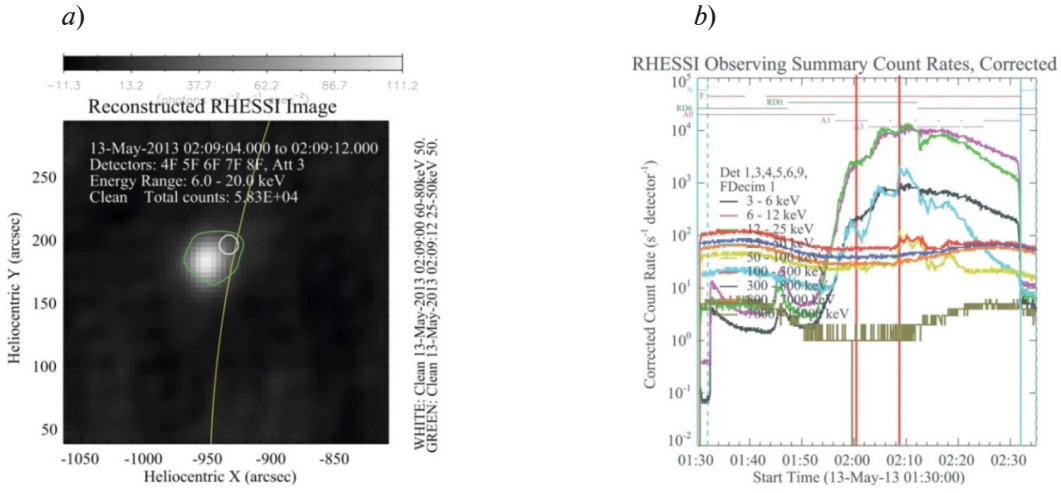

Fig. 1. X-ray image of the flare at 02:09:04 UT, white color - CLEAN 50% contour 6-20 keV, green color 50% contour 25-50 keV, white color 50% contour 60-80 keV, yellow line - Solar limb (*a*) time profile of the flare SOL2013-05-13T02:12 based on RHESSI data, red vertical lines indicate time intervals, which will be analyzed further (*b*)

X-ray spectra: models of thick and thin targets

Thick target approximation describes the case in which electrons lose all their energy in a hard X-ray source. Thus, at each moment of time, the source contains energetic electrons not only with the injection spectrum, but also with all harder spectra [8].

The thin target approximation is implemented in the case when electrons pass through a small depth, and spectrum changes in the source of hard X-ray radiation can be neglected. Intermediate cases could be described by the characteristic depth of the target or by the characteristic time for electrons to leave the region. The paper [15] gives the following relations for characteristic times: τ_e is exit time, τ_c is Coulomb collision time, τ_i is continuous injection time.

$$\tau_c \leq \tau_e \leq \tau_i \text{ for thick target approximation}$$

$$\tau_e \leq \tau_c \leq \tau_i \text{ thin target approximation.}$$

X-ray spectra

According to the observed spectra and flux power, the flare was nominally divided into two phases: before the main peak and after the main peak in energies ranges 25–50, 50–100 keV (02:08:08) (Fig. 1,*b*). Below are examples of representative spectra from each phase and their analysis (Figs. 2, 3).

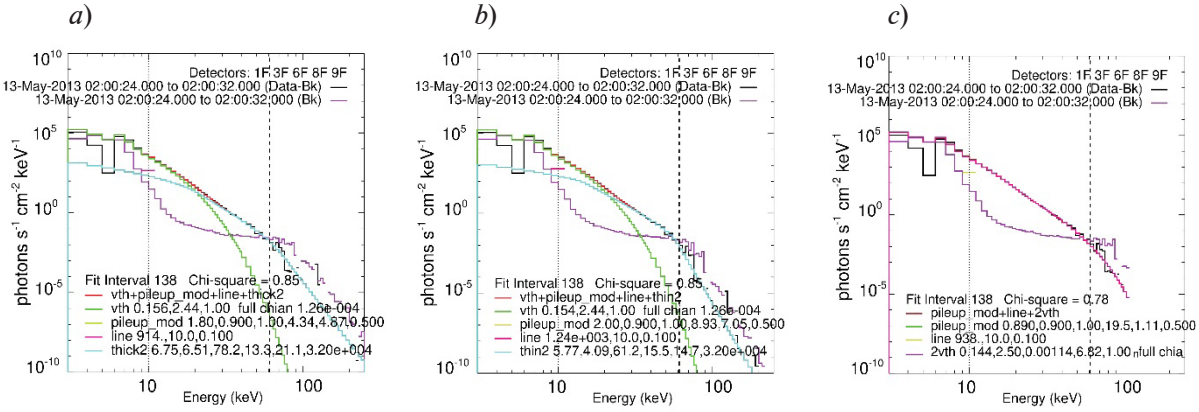

Fig. 2. Three different fitting models for the spectrum at 02:00:24-02:00:32 (before the main peak) vth+pileup_mod+line+thick2 (*a*), vth+pileup_mod+line+thin2 (*b*), 2vth+pileup_mod+line (*c*). Fitting models names according to Object Spectral Executive (OSPEX) [16] package functions in SolarSoft IDL software [17]

Before the main peak, the spectrum extends up to 50–60 keV; after the peak, a characteristic spectrum flattening at 40-100 keV appears in the spectrum, associated with the emission of non-thermal accelerated electrons. For analyzing the X-ray spectrum the following models were considered: thermal radiation of a two-temperature plasma (2vth function), a combination of a thin target (thin2 function), a thick target (thick2 function) with the addition of a single-temperature model of thermal radiation (vth function), auxiliary functions representing a pile-up correction (pileup_mod function), and an instrumentally formed line at 10 keV (line Gaussian function) [18]. A significant difference in the type of spectra in above intervals leads to qualitatively different questions of choosing a fitting model for these intervals.

Before the main peak, the two-temperature plasma model makes it possible to describe the spectrum at 10–60keV by the plasma thermal radiation. This model for the specified time interval well describes spectra by plasma thermal radiation with temperatures ~28MK and ~ 80MK. We consider heating to 80MK is implausible, but do not exclude it from consideration. Therefore, we consider the models with one-temperature approximation as more physically acceptable. The emission measure in these models before the main peak is $\sim 0.15 \cdot 10^{49} \text{cm}^{-3}$. It is worth mentioning that these values of emission measure and temperature 28 MK are obtained for both models with thin and thick targets (Fig. 2, Table 1).

Table 1

Fits parameters and estimation of density for time interval 2:00:24 - 2:00:32

	chi^2	T_1 (MK)	EM (10^{49}cm^{-3})	n (cm^{-3})	T_2 (MK)	EM$_2$ (10^{49}cm^{-3})	δ_1	E_{break} (keV)	δ_2
2vth	0.78	29	0.14	$2.7\cdot10^{10}$, $3.6\cdot10^{10}$	79	0.001	-	-	-
vth+ thin2	0.85	28	0.15	$2.8\cdot10^{10}$, $3.7\cdot10^{10}$	-	-	4.1	61	14.3
vth+ thick2	0.85	28	0.16	$2.8\cdot10^{10}$, $3.8\cdot10^{10}$	-	-	6.5	78	13.3

Notations: The fitting function is the models from the first column +pileup +line 10keV. Here EM is the emission measure; two density values are obtained for the volume of the emitting region of a sphere and a cylinder, respectively; E_{break} is the break energy in the electron flux distribution; δ_1 and δ_2 are the power-law indices of the electron flux distribution function below and above E_{break}, respectively.

After the main peak there is no question about only thermal radiation, the choice of a target for describing the nonthermal part of the spectrum is required. The results for thin and thick targets are shown in Table 2, Fig. 3. The difference in the chi-square for the resulting fits is not significant and it is necessary to rely on the interpretation of physical processes and the resulting parameters of the flare plasma to distinguish between thick and thin targets. The paper [10] discusses a model of a thick warm target for the peak.

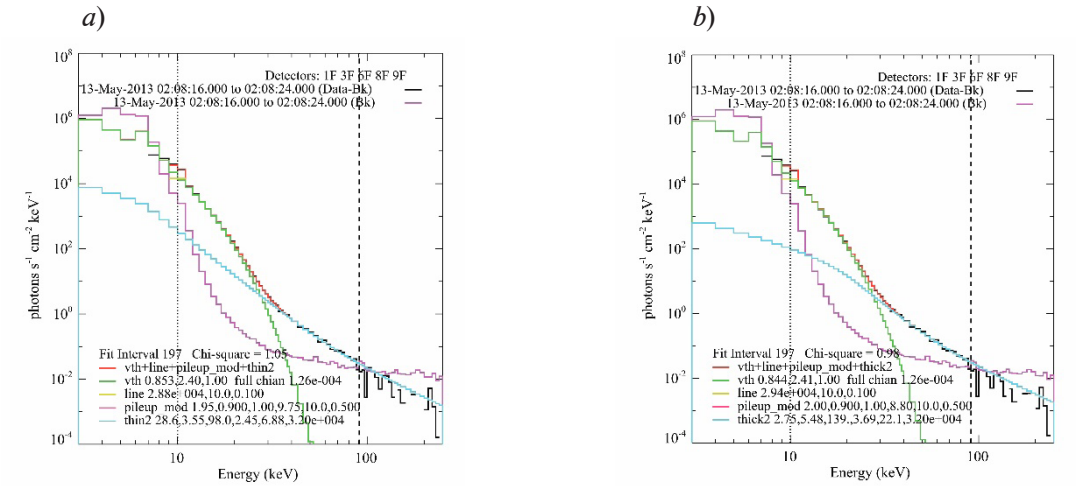

Fig. 3. Two fitting models of spectra at 02:08:16-02:08:24 (after the main peak) vth+pileup_mod+line+thin2 (*a*), vth+pileup_mod+line+thick2 (*b*)

Table 2

Fits parameters and estimation of density for interval 2:08:16 - 2:08:24

	chi^2	EM (10^{49}cm^{-3})	T (MK)	n (cm^{-3})	δ_1	E_{break} (keV)	δ_2
vth+thin2	1.05	0.85	27.8	$6.7\cdot10^{10}$, $1.1\cdot10^{11}$	3.6	98.0	2.5
vth+thick2	0.98	0.84	28.0	$6.7\cdot10^{10}$, $1.1\cdot10^{11}$	5.5	139.0	3.7

See notations for Table 1.

X-ray source size and estimation of plasma density

Let us discuss an estimation of a volume and plasma density based on X-ray source size. Two imaging RHESSI reconstruction methods were used: CLEAN (beam factor = 1, contour level 50%), VIS FWDFIT algorithm. The uncertainty in the third invisible spatial parameter leads to an additional inaccuracy in the volume estimation. The volume of the radiating region can be estimated in different ways, assuming the region to be a sphere, a cylinder, or some other shape. Sources of different shapes were obtained by imaging methods: CLEAN makes it closer to a circle, VIS FWDFIT makes a more flattened ellipse, but the characteristic size is the same in both results (see Fig. 4). Using the results of VIS FWDFIT (Table 3), we estimate the volume of the source both as a sphere and as a cylinder.

$$V = 4/3\pi \cdot R^3,\ R = 0.5 \text{ major axis},\ V = 0.25\pi \cdot D^2 \cdot h,\ h = \text{major axis},\ D = \text{minor axis}.$$

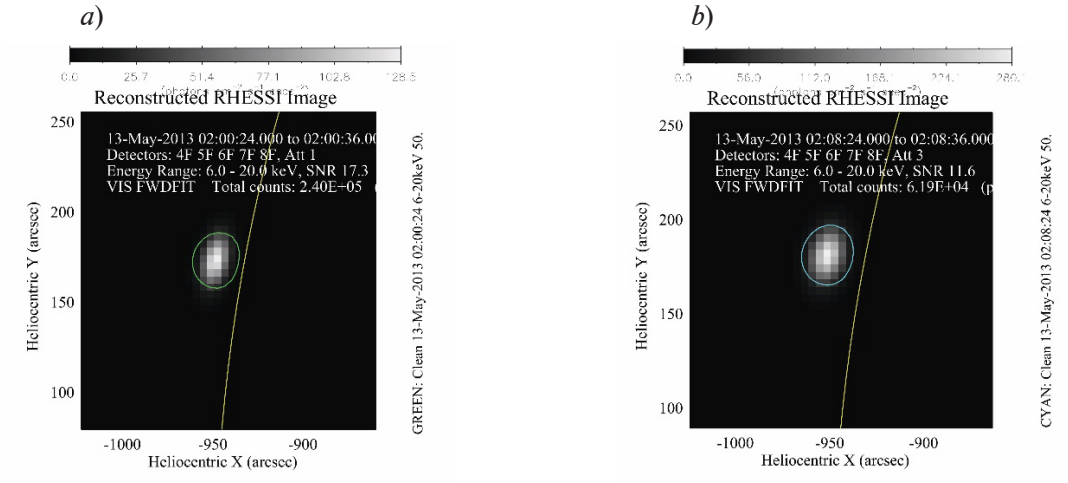

Fig. 4. X-ray images of the flare obtained by VIS FWDFIT and CLEAN methods for two time intervals from different phases of the flare: 2:00:24-2:00:36 (before the main peak) (*a*), 2:08:24-2:08:36 (after the main peak) (*b*)

Table 3

Source size by VIS FWDFIT and estimation of volume, density and E_{stop}

	major axis (arcsec)	minor axis (arcsec)	V_{sphere} (cm^3)	$V_{cylinder}$ (cm^3)	n_{min} (cm^{-3})	n_{max} (cm^{-3})	E_{stop1} (keV)	E_{stop2} (keV)
2:00:24	21.5 ± 0.5	13.2 ± 0.4	(2.0±0.1) 10^{27}	(1.12±0.08) 10^{27}	$2.7 \cdot 10^{10}$	$3.6 \cdot 10^{10}$	15	17
2:08:24	21.2 ± 0.3	10.5 ± 0.2	(1.9±0.1) 10^{27}	(0.69±0.03) 10^{27}	$6.5 \cdot 10^{10}$	$1.1 \cdot 10^{11}$	23	30

For the obtained values, we determine the plasma density $n = (EM \cdot V^{-1})^{1/2}$. The values of the emission measure of thin and thick targets are close, so we do not consider these models separately while finding the plasma parameters. We estimate the minimum and maximum values of density using estimation of volume as a sphere and as a cylinder. Next, E_{stop} is determined as the energy of electrons that lose all their energy due to Coulomb interactions with ions of the surrounding plasma. E_{stop1} and E_{stop2} were obtained using n_{min}, n_{max} respectively.

$$E_{stop} = (4\pi \cdot n \cdot e^4 \cdot \Lambda_k \cdot l)^{1/2},$$

where e is elementary charge, n is plasma density, Λ_k is the Coulomb logarithm, l is size of a region. VIS FWDFIT estimated size of a region estimated as a major axis of ellipse (Table 3).

For electrons with energies less than E_{stop}, the thick target approximation is applicable in the radiation region. The results are shown in table 3. The obtained plasma parameters indicate the choice of a thin target model for this event in the energy range > E_{stop}.

Summary

The X-ray emission of the SOL2013-05-13T02:12 X1.7-GOES-class flare was analyzed. Before the main peak spectrum was described by the plasma thermal radiation with temperatures 28 MK and 80MK. We consider heating to 80MK is implausible. Spectra could also be represented by models with thin and thick targets before the main peak and after. Worth to mention these approximations are boundary cases in the propagation of high-energy electrons in flare plasma, and might not fully describe the ongoing processes. Thus, intermediate cases are most likely to be implemented. For obtained parameters emission measure, plasma density, source size, volume of emitting region and E_{stop} we evaluated applicability of thin and thick approximations for fixed energy range. Note that, regardless of the choice of the target model, temperature of plasma and emission measure change insignificantly.

The value of E_{stop} mainly depends on the correctness of determining the size of the source and on the unknown filling factor. Let us take a filling factor of 1. Then, before the peak, since the region of transition from thermal to nonthermal radiation is higher than E_{stop} (see Fig. 2, Table 3), nonthermal radiation with energies >20keV could be considered as corresponding to a thin target with parameters indicated in table 1. In case after the peak phase the characteristic energy of transition from a thermal to a nonthermal radiation is also near the ~E_{stop} during this phase, namely between 23–30 keV. Therefore after the peak the thin target model is also applicable to the nonthermal radiation >30 keV.

REFERENCES

1. **Zharkova V.V., Arzner K., Benz A.O., et al,** Recent Advances in understanding particle acceleration processes in solar flares, Space Science Reviews, 159 (1–4) (2011) 357–420.

2. **Somov B.V., Syrovatskii S.I.,** Physical processes in the solar atmosphere associated with flares, Uspekhi Fizicheskih Nauk, 120 (10) (1976) 217.

3. **Filatov L.V., Melnikov V.F.,** Microwave Emission of a Flare Loop in the Presence of Whistler Turbulence, Geomagnetism and Aeronomy, 60 (8) (2020) 1137–1145.

4. **Shabalin A.N., Ovchinnikova E.P., Globina V.I., Charikov Y.E.,** Accelerated Electron Propagation Model for the Flare Arcade of the September 23, 2014, Event from RHESSI, SDO, and Nobeyama Radioheliograph Observations, Geomagnetism and Aeronomy, 59 (8) (2019) 1128–1138.

5. **Fisher G.H., Canfield R.C., McClymont A.N.,** Flare Loop Radiative Hydrodynamics - Part Six - Chromospheric Evaporation due to Heating by Nonthermal Electrons , The Astrophysical Journal, 289 (1985) 425.

6. **Liu W., Petrosian V., Mariska J.T.,** Combined modeling of acceleration, transport, and hydrodynamic response in solar flares. I. the numerical model, Astrophysical Journal, 702 (2) (2009) 1553–1566.

7. **Karlicky M., Barta M.,** X-Ray Loop-Top Source Generated by Processes in a Flare Collapsing Trap, The Astrophysical Journal, 647 (2) (2006) 1472–1479.

8. **Brown J.C.,** The deduction of energy spectra of non-thermal electrons in flares from the observed dynamic spectra of hard X-ray bursts, Solar Physics, 18 (3) (1971) 489–502.

9. **Brown J.C., Emslie A.G.,** Analytic limits on the forms of spectra possible from optically thin collisional bremsstrahlung source models, The Astrophysical Journal, 331 (1988) 554.

10. **Kontar E.P., Jeffrey N.L.S., Emslie A.G.,** Determination of the Total Accelerated Electron Rate and Power Using Solar Flare Hard X-Ray Spectra , The Astrophysical Journal, 871 (2) (2019) 225.

11. **Syrovatskii S.I., Shmeleva O.P.,** Nagrev plazmy bystrymi elektronami i neteplovoe rentgenovskoe izluchenie pri solnechnyh vspyshkah [Plasma heating by fast electrons and nonthermal X-ray emission during solar flares], Astronomicheskii Zhurnal 49 (1972) 334-347.

12. **Lin R.P., Dennis B.R., Hurford G.J., et al,** The Reuven Ramaty High-Energy Solar Spectroscopic Imager (Rhessi), Solar Physics, 210 (1/2) (2002) 3–32.

13.**Lemen J.R., Title A.M., Akin D.J., et al ,** The Atmospheric Imaging Assembly (AIA) on the Solar Dynamics Observatory (SDO), Solar Physics, 275 (1–2) (2012) 17–40.

14. **Effenberger F., da Costa F.R., Oka M., et al,** Hard X-Ray Emission from Partially Occulted Solar Flares: RHESSI Observations in Two Solar Cycles, The Astrophysical Journal, 835 (2) (2017) 124.

15. **Somov B.V., Syrovatskii S.I.,** Physical processes in the solar atmosphere associated with flares, Uspekhi Fizicheskih Nauk, 120 (10) (1976) 217.

16. OSPEX. URL:http://hesperia.gsfc.nasa.gov/rhessidatacenter/spectroscopy.html
17. SolarSoft IDL software. URL: http://www.lmsal.com/solarsoft/
18. **Phillips K.J.H., Chifor C., Dennis B.R.,** RHESSI Observations of the Solar Flare Iron-Line Feature at 6.7 keV, The Astrophysical Journal, 647 (2) (2006) 1480–1490.

THE AUTHOR

OVCHINNIKOVA Evgeniia P.
elfimovaevgeniya@gmail.com
ORCID: 0000-0001-7892-093X

Received 02.11.2022. Approved after reviewing 10.11.2022. Accepted 10.11.2022.